Ionic Liquids and Electrolytes with Flexible Aromatic Anions

Citation for the original published paper (version of record):
Ahmed, M., Bhowmick, S., Filippov, A. et al (2023). Ionic Liquids and Electrolytes with Flexible Aromatic Anions. Chemistry - A European Journal, 29(41).
http://dx.doi.org/10.1002/chem.202301000

Chemistry–A European Journal
Research Article
doi.org/10.1002/chem.202301000
Chemistry Europe
European Chemical Societies Publishing
www.chemeurj.org

Ionic Liquids and Electrolytes with Flexible Aromatic Anions

Special Collection

Mukhtiar Ahmed,[a] Sourav Bhowmick,[a] Andrei Filippov,[a] Patrik Johansson,*[b] and Faiz Ullah Shah*[a]

Abstract: Five new *n*-tetrabutylphosphonium $(P_{4444})^+$ cation-based ionic liquids (ILs) with oligoether substituted aromatic carboxylate anions have been synthesized. The nature and position of the oligoether chain affect thermal stability (up to 330 °C), phase behaviour ($T_g < -55$ °C) and ion transport. Furthermore, with the aim of application in lithium batteries, electrolytes were created for two of the ILs by 10 mol% doping using the corresponding Li-salts. This affects the ion diffusion negatively, from being higher and equal for cations and anions to lower for all ions and unequal. This is due to the stronger ionic interactions and formation of aggregates, primarily between the Li^+ ions and the carboxylate group of the anions. Electrochemically, the electrolytes have electrochemical stability windows up to 3.5 V, giving some promise for battery application.

Introduction

The immense need for electrochemical energy storage is today largely fulfilled by rechargeable lithium-ion batteries (LIBs) due to their high energy density, low cost, and stable cyclability,[1–3] Yet, the conventional liquid electrolytes employed have some fundamental safety issues[4,5] being based on lithium hexafluorophosphate ($LiPF_6$), which decomposes at elevated temperatures, producing *e.g.* highly toxic hydrofluoric acid (HF) and organo-phosphorous compounds,[6–8] dissolved in highly flammable carbonate-based organic solvents. Today, the field of LIB R&D urges for electrolytes that are non-flammable and both thermally and electrochemically stable in order to intrinsically improve the safety.[9–11]

Ionic liquid (IL) based electrolytes is one route pursued, which uses the fact that ILs offer wide liquidus ranges, high thermal stabilities, negligible volatilities, and are non-flammable – hence promising with respect to safety.[12,13] The most commonly studied IL-based electrolytes for LIBs are made by dissolving either lithium bis(trifluoromethanesulfonyl)imide (LiTFSI)[14,15] or lithium bis(fluorosulfonyl)imide (LiFSI)[16] in an IL of the same anions and well-known cations such as phosphonium,[17] pyrrolidinium,[18] imidazolium,[19] morpholinium[20] or piperidinium.[21] The use of these fluorinated anions is, however, less desirable due to their sensitivity to moisture, corrosion of current collectors, and potential health and environmental risks during both production and recycling.[22–24]

The anion also plays an important role in the overall physicochemical and electrochemical properties, including the mobility of the Li^+ ions – *via* ion-ion and other interactions.[25] While many studies of IL-based electrolytes have been reported during the last two decades,[26–28] most use commercially available ILs[29] and only few new anions have been reported.[30–34] Here we present a new class of fluorine-free ILs and their corresponding electrolytes based on anions with aromatic centre and different oligoether chains. The use of a carboxylate group alongside an ether oxygen atoms containing chain, make these anions mimic the organic solvents commonly used in LIBs, such as glymes,[35–37] and carbonates,[38,39] but with the idea of the advantageous IL properties added in the design – and therefore systematic correlations between anions/ILs and key physicochemical properties are developed, with an emphasis on the ion transport and usefulness as battery electrolyte components.

Results and Discussion

We start with outlining the synthesis and structural characterization of both the ILs and the electrolytes, followed by assessing their phase and thermal behaviour, before discussing LIB-relevant performance parameters such as ionic conductivity,

[a] M. Ahmed, S. Bhowmick, A. Filippov, F. U. Shah
Chemistry of Interfaces
Luleå University of Technology
97187 Luleå (Sweden)
E-mail: faiz.ullah@ltu.se
Homepage: http://www.ltu.se/staff/f/faisha-1.31372?l=en

[b] P. Johansson
Materials Physics, Department of Physics
Chalmers University of Technology
41296 Gothenburg (Sweden)
E-mail: patrik.johansson@chalmers.se
Homepage: http://www.chalmers.se/en/persons/jpatrik/

Supporting information for this article is available on the WWW under https://doi.org/10.1002/chem.202301000

Special Collection Part of a Special Collection celebrating the 140th anniversary of the Swedish chemical society.

electrochemical stability, and ion diffusion. Finally, the coordination and ion–ion interaction aspects are discussed with the help of FTIR spectroscopy data.

Synthesis and characterization

A multistep synthetic protocol was used to create the ether functionalized aromatic acids, which are then further converted to ILs – whereof a brief description is provided below. First, tosylation of the alcohols was performed by using 4-toluenesulfonyl chloride (TsCl) to make them better alkylating agents (Scheme 1a). Second, the tosylated alcohols were reacted with aromatic methyl esters in the presence of a mild base i.e; K_2CO_3 using acetonitrile (MeCN) as a reaction medium to obtain the ether functionalized ethylsalicylates, which subsequently are further converted into their corresponding acids *via* ester hydrolysis (Scheme 1b). Finally, the acids were converted to ILs through a simple neutralization reaction with *n*-tetrabutylphosphonium hydroxide. The corresponding Li-salts were synthesized by direct neutralization of the acids with $LiHCO_3$ in aqueous medium.

The chemical structures of all the ILs (Figure 1) agree well with the mass spectrometric data and the multinuclear (^{1}H, ^{13}C and ^{31}P) NMR spectroscopic analysis. The ^{1}H and ^{13}C NMR spectra of the intermediate compounds showed all the characteristic resonance lines as presented in Figures S5–14. The ^{1}H NMR spectra of the ILs show characteristic resonance lines for the methylene protons of the ether chains in the anions in the range from 3.5 to 4.3 ppm. The absence of the broad resonance line for the acidic proton and the appearance of resonance lines at 0.90–1.0 ppm for the terminal methyl groups, the multiplet 1.46–1.54 ppm for the methylene protons, and another multiplet 2.39–2.46 ppm for the aliphatic alkyl

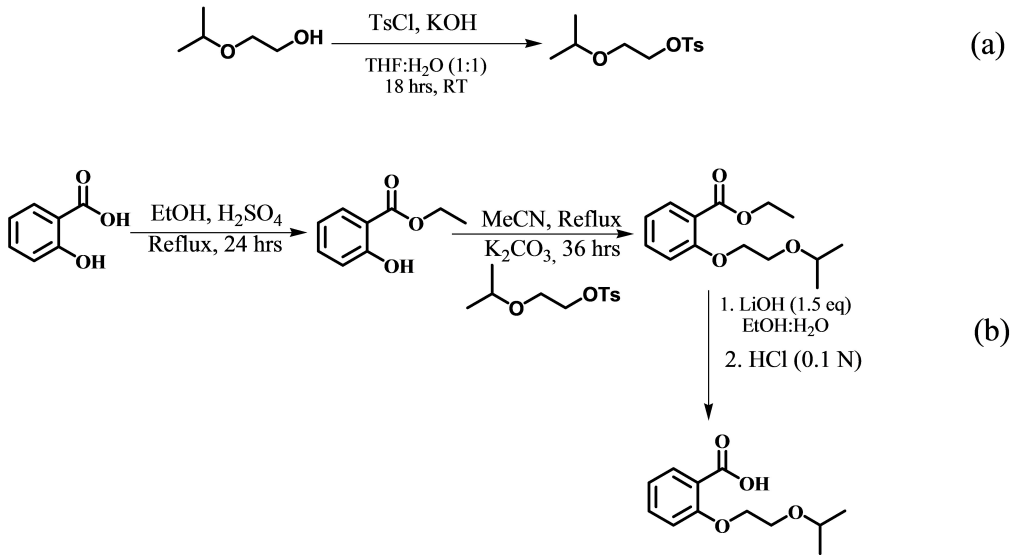

Scheme 1. (a) Tosylation of *iso*-propoxy ethanol (2-IE), and (b) Synthesis of 2-(2-isopropoxyethoxy)benzoic acid (2-IEBA).

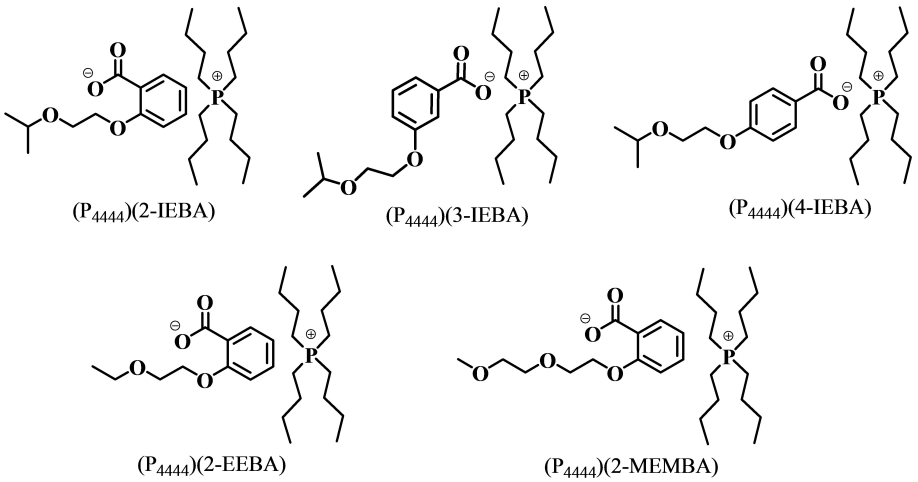

Figure 1. Chemical structures and abbreviations of the ILs.

chains attached to the $(P_{4444})^+$ cation corroborated the successful deprotonation of the corresponding acids and formation of the ILs (Figures S15–19). The ^{13}C NMR spectra revealed resonance lines in the region 65–80 ppm attributed to the aliphatic carbon directly attached to the oxygen atoms in the ether chains of the anions (Figures S20–24). In addition, the ^{13}C resonance lines for the carboxylate groups in the anions are found in the range 167–174 ppm. Finally, the ^{31}P NMR spectra indicate single resonance lines at *ca.* 33 ppm for the phosphorous nucleus in the cation (Figures S25–29).

Thermal properties

All ILs and electrolytes show excellent dynamic thermal stability with decomposition temperatures up to 330 °C (Figure 2), with the caveat that the dynamic TGA overestimate stability and should be complimented with isothermal TGA, especially for IL-based electrolytes.[40] The (P_{4444})(3-IEBA) and (P_{4444})(4-IEBA) ILs show relatively higher thermal stabilities and one-stage decompositions. In contrast, the (P_{4444})(2-IEBA), (P_{4444})(2-EEBA) and (P_{4444})(2-MEMBA) ILs exhibit two-stage decompositions, with a major weight loss of *ca.* 70% at the first stage, which, perhaps a bit surprisingly, most probably is due to the decomposition of the $(P_{4444})^+$ cation.[41]

The lower thermal stability of the ILs with ortho-substituted anions is due to the simultaneous inductive effect of the phenolic oxygen atom directly attached to the aromatic ring and the steric effects of the attached oligoether chains. This in turn leads to a decrease in the electron density around the carboxylate groups of these anions and this to a decrease in the overall ion-ion interactions. These effects are much less pronounced both at the meta- and para-positions, and at the meta-position resonance effects also come into play, causing an increase in the polarity of the anion through a push-pull mechanism and hence increased ion-ion interactions and this correlates with the highest thermal stability of the ILs made.

Doping the neat ILs with Li-salts brings additional polarity and electrostatic interactions and further improvements in the thermal stability (Figure 2c), in agreement with the literature on IL-based electrolytes.[25] The rate of weight loss during the first decomposition step is much higher than for the second decomposition step (Figure 2b) and also much lower for the electrolytes as compared with the neat ILs (Figure 2d). Overall, the thermal stabilities of these ILs and electrolytes are considerably higher as compared to traditional organic solvent-based electrolytes[42] and quite comparable with phosphonium-based ILs containing fluorine-free anions.[25,41]

From the DSC traces of the IEBA-based ILs, the change in the position of the ether chain on the phenyl ring with respect

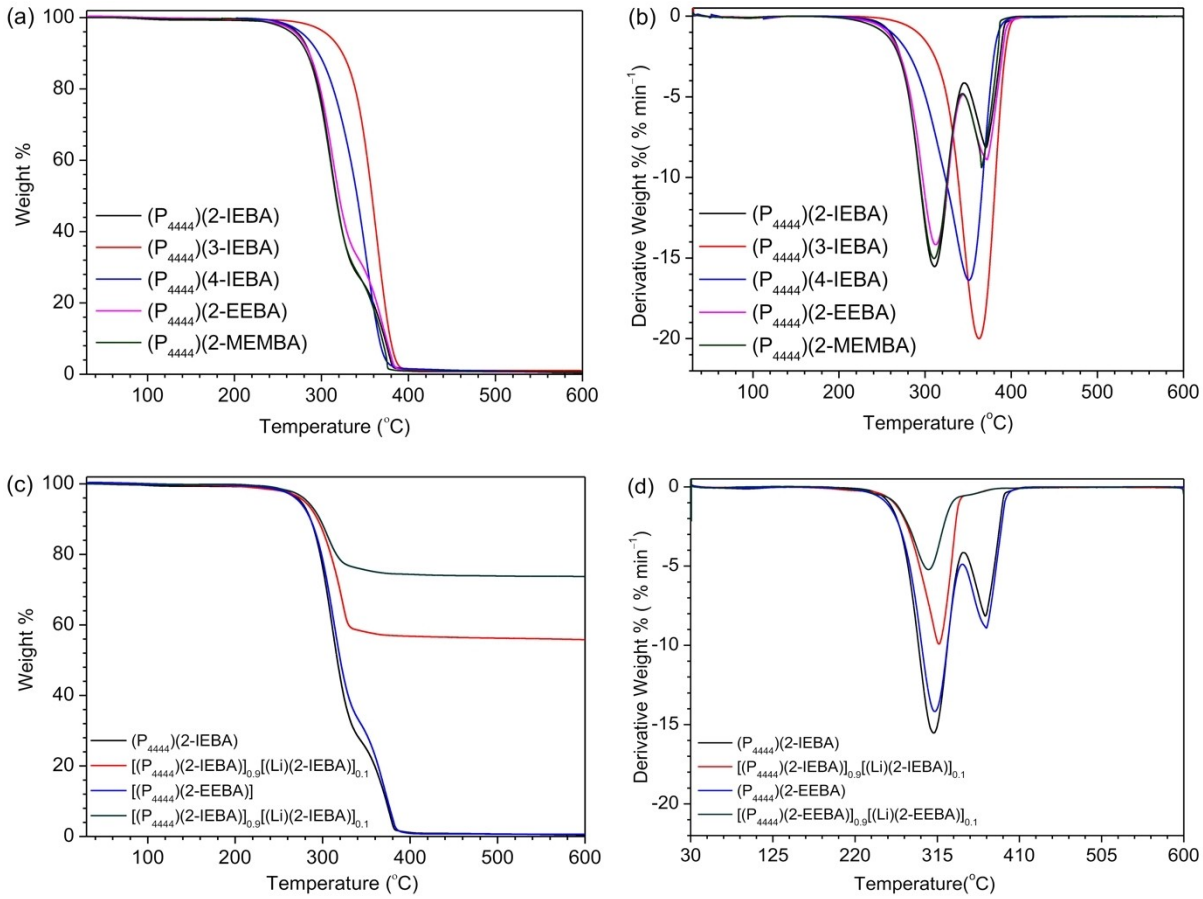

Figure 2. TGA thermograms (a and c), and DTG curves (b and d) of the ILs and the electrolytes.

to the carboxylate group clearly affects the T_g with a gradual increase from ortho to meta to para (Figure 3, Table 1). As expected due to the structural flexibility, an increase in the ethoxy units of the ether chains decreases the T_g, however, branching the ether chain leads to a slight increase. Overall, the T_gs of these ILs are higher than for the previously reported non-aromatic ether-based (P_{4444})(MEEA) IL,[25] which probably is due to the contribution of the phenyl ring, providing additional pi-pi stacking and restricting the free low energy rotations of the ether chains.[43] As expected, doping with Li-salt slightly increase the T_g, indicating some dynamic cross-linking by Li^+.[44]

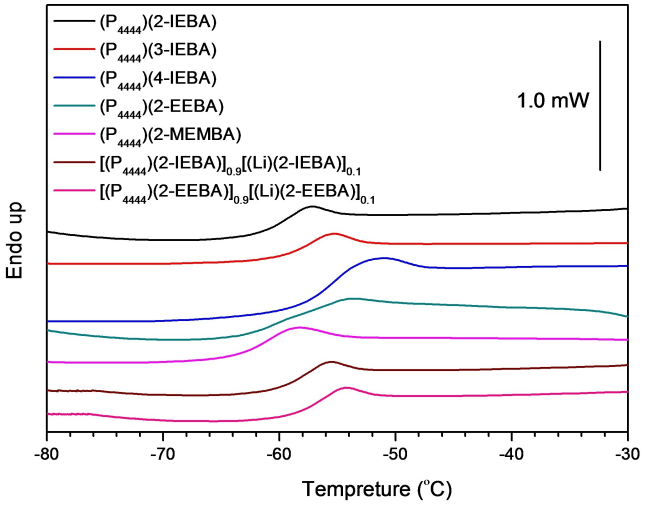

Figure 3. DSC traces for the ILs and the electrolytes. The traces are shifted along Y-axis for clarity.

Table 1. Thermal properties and ionic conductivities of the ILs and the electrolytes.

IL/Electrolyte	T_g [°C]	T_d [°C]	σ [S cm^{-1}] at 20 °C
(P_{4444})(2-IEBA)	−60	282	1.9E-4
(P_{4444})(3-IEBA)	−58	330	1.0E-4
(P_{4444})(4-IEBA)	−56	291	5.6E-5
(P_{4444})(2-EEBA)	−58	282	6.1E-5
(P_{4444})(2-MEMBA)	−62	284	6.7E-5
[(P_{4444})(2-IEBA)]$_{0.9}$ [(Li)(2-IEBA)]$_{0.1}$	−62	288	1.2E-4
[(P_{4444})(2-EEBA)]$_{0.9}$ [(Li)(2-EEBA)]$_{0.1}$	−60	289	5.5E-5

Ionic conductivity

Turning to more battery related properties, the ionic conductivity is affected by changing the position of the ether functionality to a larger extent than by changing length of the ether functional group (Figure 4, Table S1). The (P_{4444})(2-IEBA) IL with its ortho substitution on the anion shows the highest conductivity, which is attributed to reduced ion-ion interactions by the repulsion between the terminal isopropyl group of the $(2\text{-IEBA})^-$ anion and alkyl chains of the $(P_{4444})^+$ cation. Similarly, the para-substituted (P_{4444})(4-IEBA) IL has the lowest ionic conductivity because the ether group is far from the carboxylate group and there is no hindrance for the $(P_{4444})^+$ cation to approach the $(4\text{-IEBA})^-$ anion. The (P_{4444})(2-EEBA) IL with a shorter ether chain provide comparable ionic conductivity to the (P_{4444})(2-MEMBA) IL with a slightly longer ether chain, which is in accordance with the previous findings for ether functionalized cation-based ILs.[45] The addition of Li-salt lead to a slight decrease in the ionic conductivity, which is primarily due the reduction of free volume as a result of stronger electrostatic interactions (Figure 4b), but also the creation of triplets with multiple anions as well as dynamic cross-linking.

In more detail, the VFT analysis show that the E_σ for the IEBA-based ILs decreases as (P_{4444})(4-IEBA) > (P_{4444})(3-IEBA) > (P_{4444})(2-IEBA) (Table S1), in accordance with the DSC data. It is also clear that the number of charge carriers, reflected by σ_0, increases by adding Li-salts to the ILs. As expected, the T_0 obtained are *ca.* 60 K lower than the T_g obtained from the DSC data, which is in accordance with the empirical approximation for IL-based electrolytes: $T_0/T_g \approx 0.75$.[46]

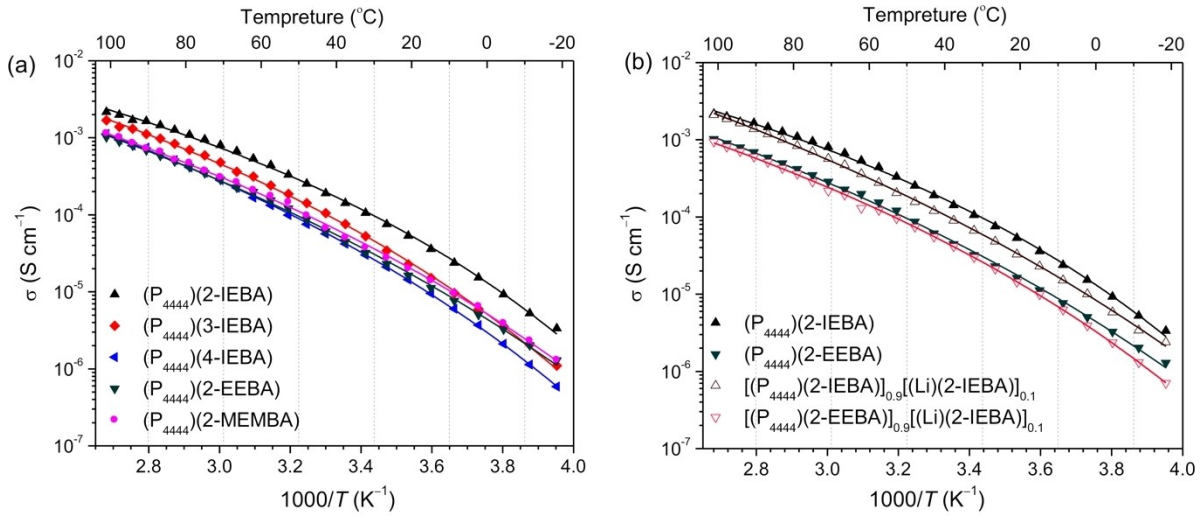

Figure 4. Ionic conductivity of the ILs (a) and the electrolytes (b) as function of temperature. The solid lines indicate best fit of the data to the VFT equation.

Electrochemical stability

For the electrochemical stability and first of all the cathodic part, all ILs and electrolytes reveal continuous reduction below 1 V *vs* Li/Li^+ (Figure 5, Table 2), which can be correlated to the presence of acidic alpha methylene protons in the phosphonium cation.[42,47–49] Yet, (P_{4444})(3-IEBA) shows somewhat improved cathodic stability as compared with the other ILs, which again might be related to the electron donating effect of the oxygen atom towards the carboxylate group *via* a resonance effect. In the anodic part, the IL anions oxidizes between 3.5–4.0 V *vs.* Li/Li^+ and the on-set is a function of the number of ethoxy units in the chain.

Both the ILs and the electrolytes based on (P_{4444})(2-IEBA) and (P_{4444})(2-EEBA) have slightly narrower ESWs – with the oxidation arguably due to the ethoxy groups present in the anion.[25] In addition, two pronounced peaks C_1 and C_2 observed in the cathodic scan, at 1.30 and 0.75 V *vs.* Li/Li^+, which can be associated with underpotential deposition (UPD) of lithium as well as partial decomposition of the $(P_{4444})^+$ cations on the GC electrode.[50,51] The UPD layer formation can modify the nature of the GC WE surface, which is beneficial for extending the cathodic limit of the electrolytes, whereas the Li^+ ions can pass and prevent further reduction of the $(P_{4444})^+$ cation.

The reversibility and long-term electrochemical stability is further assessed by cyclic voltammetry (CV) data (Figures S30). The three cycles at a slower scan rate (1 mV s^{-1}) and the hundred cycles at a higher scan rate (100 mV s^{-1}) of the $[(P_{4444})(2\text{-EEBA})]_{0.9}[(Li)(2\text{-EEBA})]_{0.1}$ electrolyte confirmed the reversibility and long-term electrochemical stability. Overall, the ESWs (*ca.* 3.14–3.57 V) are comparable with the commonly studied imidazolium-[52] and phosphonium[53]-based ILs with TFSI and other fluorinated anions. A caveat is that all these ESWs should be regarded as the upper limits as we are utilizing LSV data and the ILs and the electrolytes are highly viscous at room temperature.

Table 2. Cathodic and anodic limits and ESWs of the ILs and the electrolytes at 20 °C using GC as WE. The limits are determined by a 0.1 mA cm^{-2} cut-off current density.

IL/Electrolyte	E_C (V vs. Li/Li^+)	E_A (V vs. Li/Li^+)	ESW
(P_{4444})(2-IEBA)	0.53	3.85	3.32
(P_{4444})(3-IEBA)	0.40	3.89	3.49
(P_{4444})(4-IEBA)	0.88	4.01	3.13
(P_{4444})(2-EEBA)	0.43	4.02	3.59
(P_{4444})(2-MEMBA)	1.12	4.20	3.08
$[(P_{4444})(2\text{-IEBA})]_{0.9}$ $[(Li)(2\text{-IEBA})]_{0.1}$	0.42	3.89	3.47
$[(P_{4444})(2\text{-EEBA})]_{0.9}$ $[(Li)(2\text{-EEBA})]_{0.1}$	1.39	3.68	2.29

NMR diffusometry

The diffusion coefficients of all species show monotonous increases as function of temperature, and all also follows VFT behaviour (Figure 6a, Table S2). For all the ILs the self-diffusion coefficients of the cations (D_{cation}) and the anions (D_{anion}), as measured by ^1H NMR spectroscopy, are approximately same and cannot be separated, which is expected as they are of comparable size. The D_{cation} was also measured by ^{31}P NMR spectroscopy (Figure 6b), which corroborate this picture.

The addition of Li-salt decreases the diffusivity of both cations and anions (Figures 6c and 6d), due to additional electrostatic interactions. The diffusivity of the cations is suppressed to a larger extent than the anions, which is rather unexpected as the Li^+ cations in general interact with the IL (and salt) anions,[25] but at the same time Li^+ diffuses the slowest by virtue of triplets and larger aggregates forming.

The large differences in the VFT fits between ILs and electrolytes (Figure 6 and Table S2) can be understood by the free volume available,[54] decreasing upon Li-salt doping, which also increases the ion-ion interactions, manifested as slightly changed apparent activation energies, E_D, as well as in D_0. As a sidenote, the T_0 obtained from the ionic conductivity data are lower than the T_0 obtained from the diffusivity data; this as the latter is an average of the diffusion coefficients of isolated, paired, and clustered ions, regardless of charge, whereas the former only has contributions from charged species.

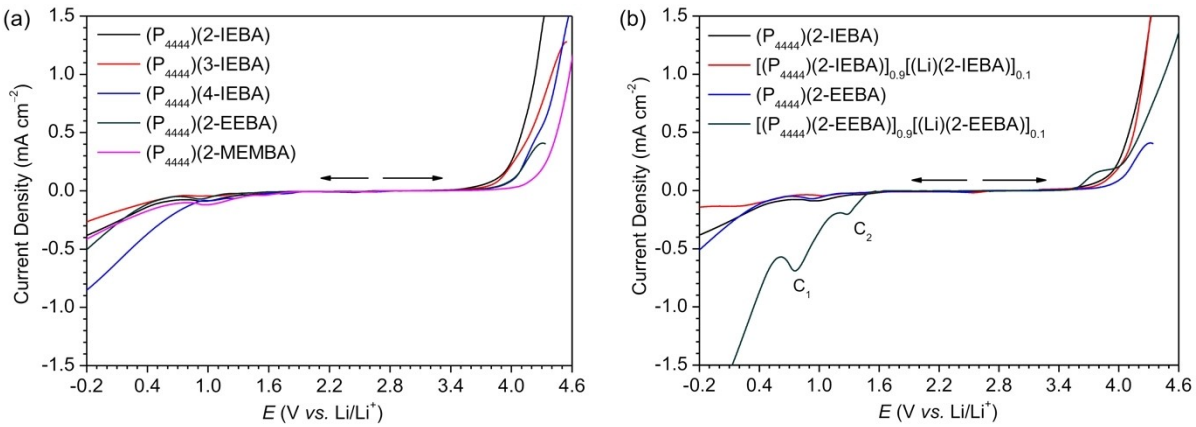

Figure 5. LSV curves of the ILs (a) and the electrolytes (b) using GC as WE at 20 °C.

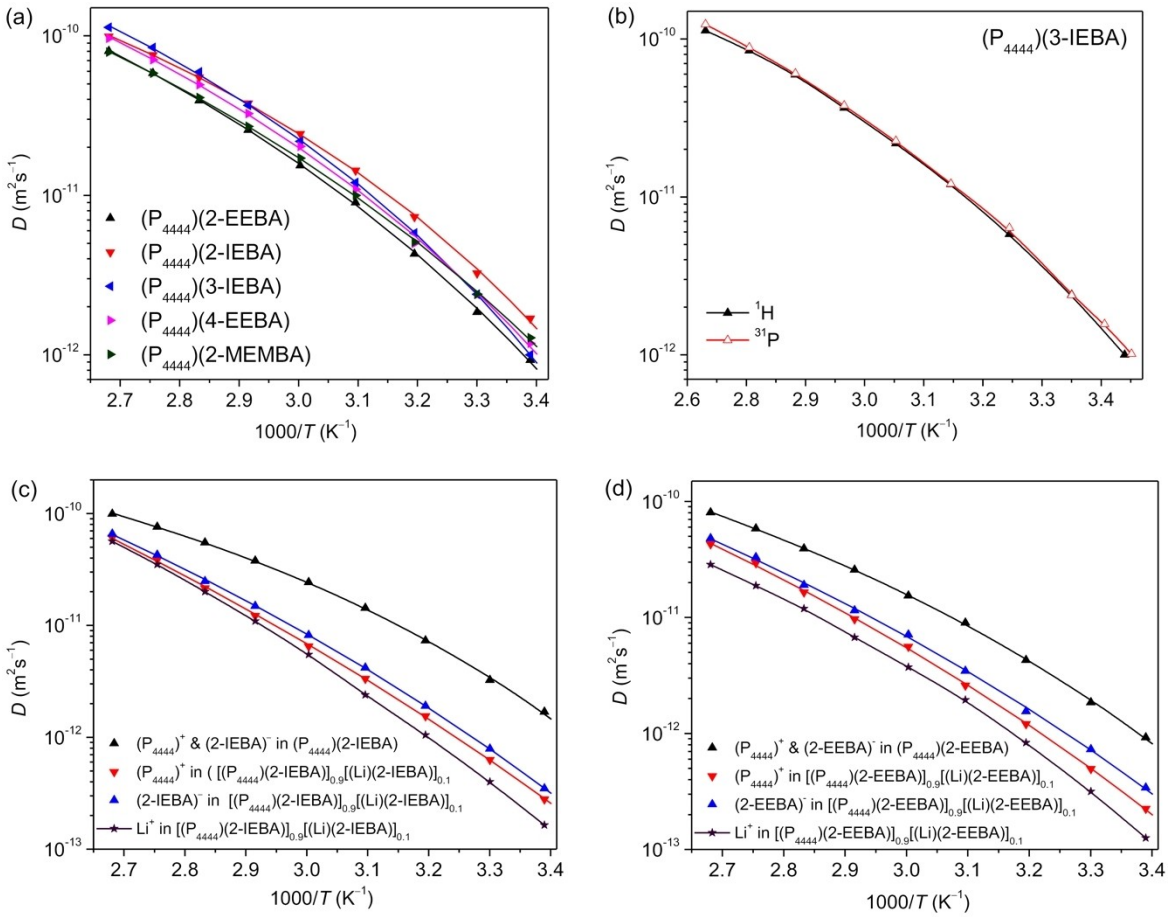

Figure 6. Diffusion coefficients of ions: (a-b) the neat ILs, and (c-d) the neat ILs and the electrolytes measured by ^{1}H (a-d), ^{31}P (b) and ^{7}Li (c-d) NMR spectroscopy. Symbols indicate experimental data and the solid lines represent the VFT fits.

In order to further compare the diffusivity of the ions in the electrolytes, the apparent transference numbers t_i for each ion were calculated from their diffusion coefficients D_i using the following Equation (1):[55,56]

$$t_i = \frac{x_i D_i}{\Sigma_i x_i D_i} \quad (1)$$

where x_i is the molar fraction of each ion. The anion t_i is higher than for both the $(P_{4444})^+$ cation and the Li^+ cation (Figure 7). The latter has the smaller contribution, which is expected due to being only 10 mol%, but is likely also affected by the formation of aggregates. PFG NMR diffusometry, however, fundamentally underestimate the diffusion coefficients of charged species and therefore the t_i of Li^+ cations determined by electrochemical techniques can be 2–3 times larger.[57]

Infrared spectroscopy

Focusing on the asymmetric and symmetric stretching of the carboxylate group, the C–O stretching and the CH_2 rocking bands of the anions, the ILs all have the former appearing as a broad band at *ca.*1595 cm^{-1} with distinct satellite bands on both sides, indicating several types of coordination sites/interactions, whereas in contrast the symmetric stretching band appears as a single broad peak at *ca.* 1380 cm^{-1}, both thus indicative of carboxylate-cation interactions (Figure 8).[58] The symmetric stretching bands for both the (P_{4444})(3-IEBA) and (P_{4444})(4-IEBA) ILs shift slightly towards higher wavenumbers as compared to (P_{4444})(2-IEBA), which likely is due to an electronic effect of the phenolic oxygen (Figure 8a).

The C–O stretching region, 800–1200 cm^{-1}, contains two main bands: one at 1093 cm^{-1} (asymmetric stretching) and one at 920 cm^{-1} ((symmetric stretching combined with CH_2 rocking) (Figure 8b).[59] For the latter the distinct shoulders found for both (P_{4444})(2-IEBA) and (P_{4444})(2-MEMBA) indicate interactions of the ethoxy units of these anions with the aliphatic protons of the $(P_{4444})^+$ cation.

As was expected, doping with Li-salt changes the interactions and thus the spectra; the peak at 1595 cm^{-1} split into two distinct bands, confirming strong Li^+- carboxylate group interactions, and similar changes are seen in the symmetric stretching band at 1380 cm^{-1} (Figure 8c). In contrast, there are minimal changes in the lower wavenumber regions, indicating

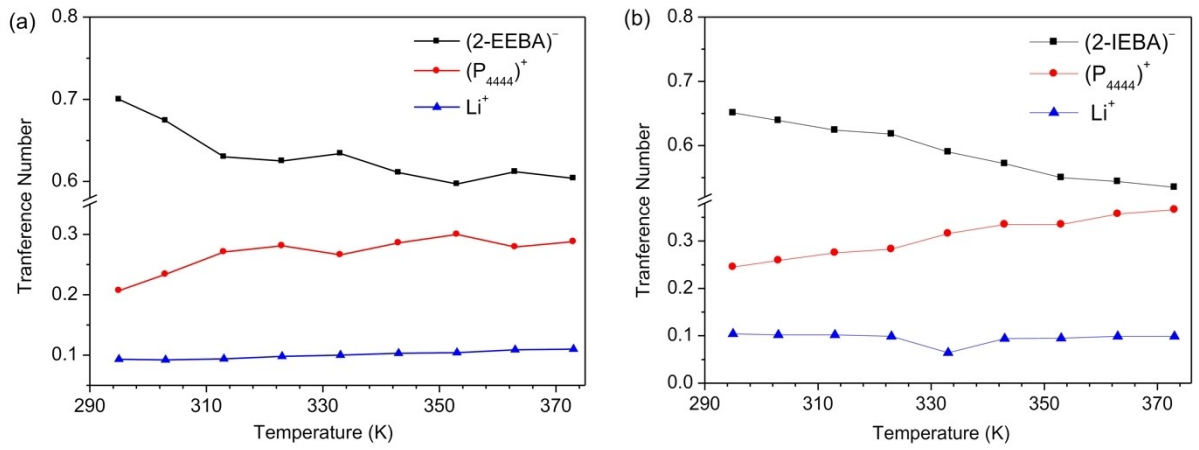

Figure 7. Apparent transfer numbers in the (a) $[(P_{4444})(2\text{-EEBA})]_{0.9}[(Li)(2\text{-EEBA})]_{0.1}$ and $[(P_{4444})(2\text{-IEBA})]_{0.9}[(Li)(2\text{-IEBA})]_{0.1}$ electrolytes as calculated from the PFG NMR diffusion data.

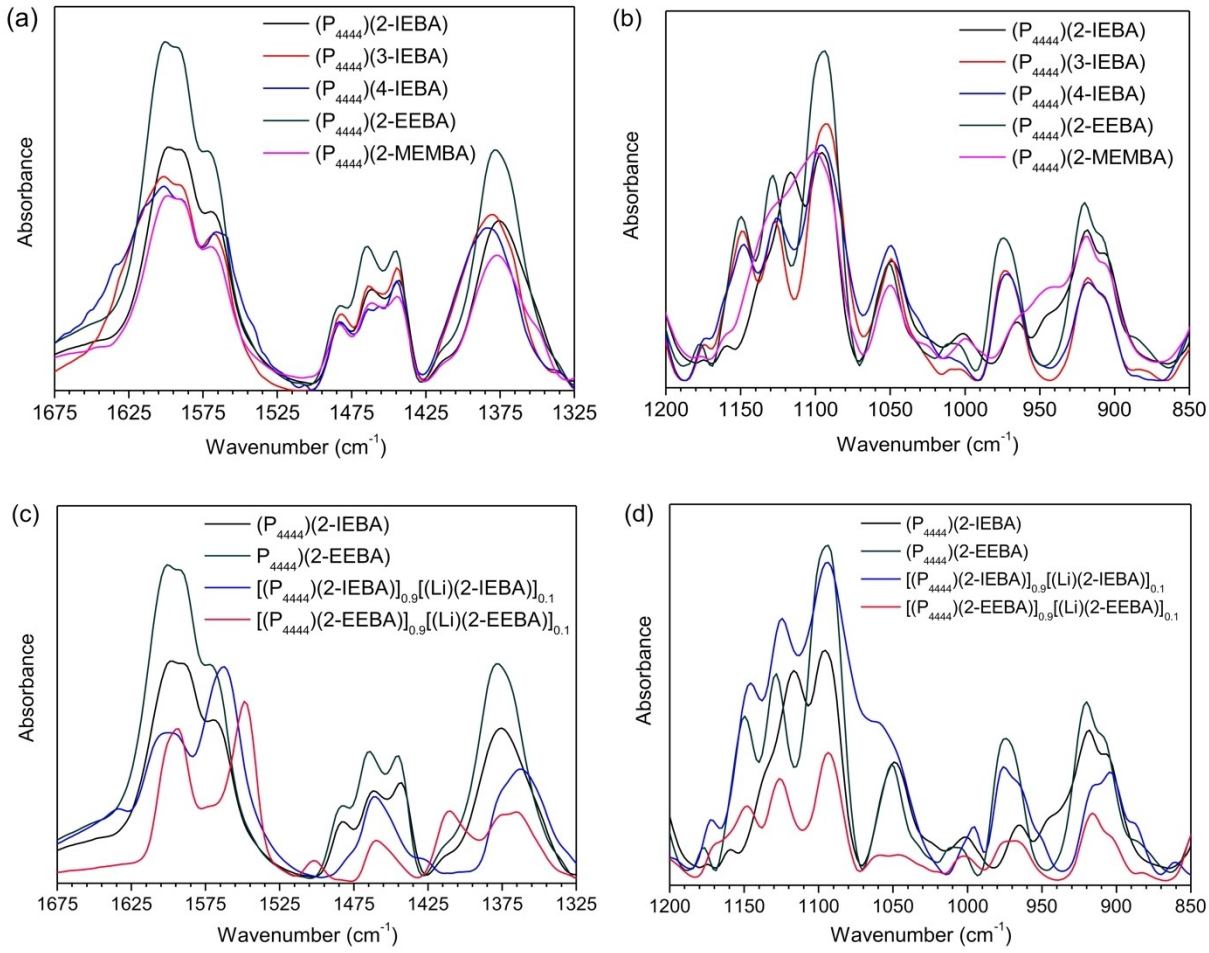

Figure 8. FTIR spectra of the ILs (a and b) and the electrolytes (c and d).

weaker interactions with the ethoxy units of the ether chains (Figure 8d).

Conclusion

Despite the structural similarities, the $(P_{4444})(2\text{-IEBA})$ IL offered key beneficial properties including lower T_g, higher ionic

conductivity and higher ion diffusivity, but lower dynamic thermal stability, than both (P_{4444})(3-IEBA) and (P_{4444})(4-IEBA) ILs. As was expected, the addition of Li salt to the ILs decreased the ionic mobility and thereby lead to reduced ionic conductivity and ion diffusivity, although both the latter increase monotonically as a function of temperature. The anions diffuse faster within the electrolytes than the $(P_{4444})^+$ cations and Li^+ ions, despite the fact that the FTIR spectroscopy data revealed interactions between the Li^+ ions and the carboxylate group of the anions. Altogether, the designed ILs and the electrolytes are fluorine-free and have better physicochemical properties than conventional LIB electrolytes and have a potential to be used as electrolytes in next generation batteries operating at elevated temperatures and with limited ESWs.

Experimental Section

Materials: Unless otherwise noted, all the commercial reagents were utilized without any additional purification. Salicylic acid (ACS reagents, >95% purity), 4-toluenesulfonyl chloride (ACS reagents, >97% purity), 2-ethoxyethanol (>99% purity), *iso*-propoxy ethanol (>99% purity), diethylene glycol monoethyl ether (>99% purity), an aqueous solution of tetrabutylphosphonium hydroxide (40 wt% in water) and lithium hydroxide monohydrate (ACS reagents, >98% purity) were received from Sigma-Aldrich. Sodium sulphate (Na_2SO_4), potassium carbonate (K_2CO_3), lithium bicarbonate ($LiHCO_3$), methanol, dichloromethane (DCM), acetonitrile and diethylether were all purchased from VWR (BDH) chemicals. The water content was measured by Karl Fischer titration using Metrohm 917 Coulometer, Switzerland, placed inside a Mbraun glovebox with water and oxygen contents <0.5 ppm and was determined to be <100 ppm for all synthesized ILs and the electrolytes.

Synthesis: The synthesis procedure for 2-(2-isopropoxyethoxy)benzoic acid (2-IEBA) is described in detail, all the other acids are synthesized using the same two-step reaction procedure.

Synthesis of 2-(2-isopropoxyethoxy)benzoic Acid (2-IEBA)

Step 1: Synthesis of 2-isopropoxyethyl 4-methylbenzenesulfonate: Solution of potassium hydroxide (0.38 g, 6.9 mmol, 1.2 equiv.) in water (20 mL) was dropped into the *iso*-propoxy ethanol (0.9 g, 8.6 mmol, 1.5 equiv.) over 5 minutes and after complete addition the mixture was further stirred for 10 minutes. Solution of 4-toluenesulfonyl chloride (1.1 g, 5.7 mmol, 1 equiv.) in THF (500 ml) at room temperature was dropped into the mixture under vigorous stirring over 50 minutes and stirred at ambient temperature for further 24 hours. 250 mL of water was added to reaction mixture and extracted with DCM (3×100 mL). The organic layer was dried over Na_2SO_4, gravity filtered, and the solvent was removed by rotary evaporation, a pale-yellow liquid was obtained and used in the next step without any further purification.

Step 2: Synthesis of Aromatic Acids: A solution of 2-isopropoxyethyl 4-methylbenzenesulfonate (38.7 g, 0.15 moles, 1.5 equiv. in 100 ml of dry acetonitrile), methyl salicylate (15.2 g, 0.1 moles, 1 equiv.) and potassium carbonate (69 g, 0.5 moles, 5 equiv.) in a dry acetonitrile (250 mL) was heated at 70 °C under N_2 and continuous stringing for 48 hours. The yellow suspension was filtered off and the solid was washed with 60 mL of acetonitrile. The extract and washes were concentrated *via* rotary evaporation. The residue was extracted with DCM (3×50 mL). The organic phase was washed with water (6×150 mL). The organic layer was dried over Na_2SO_4, gravity filtered, and the solvent was removed by a rotary evaporation to afford the product ether functionalized ethylsalicylate as a yellow oil. In the next step, the product was dissolved in THF:MeOH (1:1, 50 mL) and dropped into the aqueous solution of $LiOH.H_2O$ (3 equiv.), stirred at room temperature for 12 hours, neutralized with 0.1 M HCl and extracted with DCM (3×25 mL). The organic phase was washed with water (6×150 mL), dried over Na_2SO_4, gravity filtered, and the solvent was removed by rotary evaporation to afford the product 2-(2-isopropoxyethoxy)benzoic acid (2-IEBA) as a dark yellow liquid. All the acids were separated in good yields *ca.* 60%.

2-(2-isopropoxyethoxy)benzoic acid (2-IEBA): Dark yellow liquid. ^{1}H NMR (400.21 MHz, $CDCl_3$), δ(ppm): 10.34 (*b*, 1H), 8.16–8.14 (*d*, $^3J_{HH}$=8.2 Hz 1H), 7.56–7.52 (*d*, $^3J_{HH}$=8.1 Hz, 1H), 7.11–7.03 (*t*, $^3J_{HH}$=8.3 Hz 1H), 4.37-4.34 (*t*, $^3J_{HH}$=4.3 Hz, 2H, O–CH_2–), 3.84-3.82 (*t*, $^3J_{HH}$=4.5 Hz, 2H, –CH_2–O), 3.72–3.66 (*sept*, $^3J_{HH}$=6.1 Hz, 1H, –CH), 1.21–1.20 (*d*, $^3J_{HH}$=6.1 Hz, 6H, –CH_3) ppm. ^{13}C NMR (100.64 MHz, $CDCl_3$): 171.20, 163.58, 132.43, 121.78, 114.56, 72.47, 68.12, 66.45, 22.19.

3-(2-isopropoxyethoxy)benzoic acid (3-IEBA): Dark yellow liquid. ^{1}H NMR (400.21 MHz, $CDCl_3$), δ(ppm): 11.66 (*b*, 1H), 7.73-7.71 (*d*, $^3J_{HH}$=7.6 Hz 1H), 7.66 (*s*, 1H),7.40–7.36 (*t*, $^3J_{HH}$=8.0 Hz 1H), 7.19–7.18 (*t*, $^3J_{HH}$=8.0 Hz 1H), 4.20–4.17 (*t*, $^3J_{HH}$=4.8 Hz, 2H, O–CH_2–), 3.85–3.82 (*t*, $^3J_{HH}$=4.7 Hz, 2H, –CH_2–O), 3.76–3.69 (*sept*, $^3J_{HH}$=6.7 Hz, 1H, –CH), 1.24–1.23 (*d*, $^3J_{HH}$=6.2 Hz, 6H, –CH_3) ppm. ^{13}C NMR (100.64 MHz, $CDCl_3$): 171.20, 163.58, 132.43, 121.78, 114.56, 72.47, 68.12, 66.45, 22.19.

4-(2-isopropoxyethoxy)benzoic acid (4-IEBA): Dark yellow liquid. ^{1}H NMR (400.21 MHz, $CDCl_3$), δ(ppm): 8.07–8.05 (*d*, $^3J_{HH}$=8.6 Hz, 2H), 7.99–7.97 (*d*, $^3J_{HH}$=8.6 Hz, 2H), 4.21–4.18 (*t*, $^3J_{HH}$=4.6 Hz, 2H, O–CH_2–), 3.83–3.81 (*t*, $^3J_{HH}$=5.2 Hz, 2H, –CH_2–O), 3.81–3.68 (*sept*, $3J_{HH}$=6.0 Hz, 1H, –CH), 1.24–1.22 (*d*, $^3J_{HH}$=6.1 Hz, 6H, –CH_3) ppm. ^{13}C NMR (100.64 MHz, $CDCl_3$): 171.20, 163.58, 132.43, 121.78, 114.56, 72.47, 68.12, 66.45, 22.19.

2-(2-ethoxyethoxy)benzoic acid (2-EEBA): Dark yellow liquid. ^{1}H NMR (400.21 MHz, $CDCl_3$), δ(ppm): 10.81 (*b*, 1H), 8.14–8.12 (*d*, $^3J_{HH}$=7.9 Hz 1H), 7.55–7.51 (*t*, $^3J_{HH}$=7.6 Hz, 1H), 7.13–7.11 (*d*, $^3J_{HH}$=7.5 Hz 1H), 7.10–7.03 (*t*, $^3J_{HH}$=8.3 Hz, 1H), 4.37-4.34 (*t*, $^3J_{HH}$=4.3 Hz, 2H, O–CH_2–), 3.84–3.82 (*t*, $^3J_{HH}$=4.2 Hz, 2H, –CH_2–O), 3.62–3.56 (*t*, $^3J_{HH}$=6.9 Hz, 2H, –CH_2–O), 1.25–1.21 (*d*, $^3J_{HH}$=6.9 Hz, 3H, –CH_3) ppm. ^{13}C NMR (100.64 MHz, $CDCl_3$): 165.85, 157.64, 134.93, 133.71, 122.62, 118.74, 113.75, 69.48, 67.86, 67.09, 15.03.

2-(2-(2-methoxyethoxy)ethoxy)benzoic acid (2-MEMBA): Dark yellow liquid. ^{1}H NMR (400.21 MHz, $CDCl_3$), δ(ppm): 10.91 (*b*, 1H), 8.18-8.16 (*d*, $^3J_{HH}$=8.0 Hz 1H), 7.55–7.52 (*d*, $^3J_{HH}$=8.1 Hz, 1H),7.14–7.06 (*t*, $^3J_{HH}$=8.1 Hz 1H), 4.40–4.37 (*t*, $^3J_{HH}$=4.6 Hz, 2H, O–CH_2–), 3.95-3.92 (*t*, $^3J_{HH}$=4.9 Hz, 2H, –CH_2–O), 3.64-3.62 (*t*, $^3J_{HH}$=4.3 Hz, 2H, –CH_2–O), 3.54–3.53 (*t*, $^3J_{HH}$=5.2 Hz, 2H, –CH_2–O), 1.20 (*t*, $^3J_{HH}$=5.1 Hz, 3H, –CH_3) ppm. ^{13}C NMR (100.64 MHz, $CDCl_3$): 165.71, 157.57, 134.92, 133.81, 122.65, 118.70, 113.57, 71.05, 69.93, 69.33, 68.83, 66.87, 15.23.

Synthesis of Ionic Liquids: An aqueous solution of the tetrabutylphosphonium hydroxide (13.82 g, 50 mmol) was added dropwise into the stirred aqueous solution of the acid (50 mmol in 50 ml of water). The reaction mixture was stirred at room temperature for 4 hours and progress of the reaction was monitored *via* thin layer chromatography (TLC) and upon completion of the reaction water was removed under reduced pressure using a rotary evaporator. The products were washed three times with 50 ml of diethyl ether before being dissolved in dichloromethane and dried over anhydrous Na_2SO_4. Finally, the solution was filtered, residual solvent was

removed under reduced pressure, and the final products were dried in a vacuum oven at 80 °C for more than 4 days. All the products were separated in quantitative yields.

(P_{4444})(2-IEBA): Pale yellow liquid. MS (ESI). $(C_{16}H_{36}P)^+$: Calcd m/z 259.2556. Found m/z 259.2565, $[C_{12}H_{15}O_4]^-$: Calcd m/z 223.0975, Found m/z 223.1071. ^{1}H NMR (400.21 MHz, $CDCl_3$), $^\delta$(ppm): 7.45–7.44 (*d*, $^3J_{HH}$ = 6 Hz 1H), 7.09–7.07 (*d*, $^3J_{HH}$ = 7.5 Hz, 1H), 6.85-6.82 (*m*, 2H), 4.18-4.16 (*t*, $^3J_{HH}$ = 5.6 Hz, 2H, O–CH_2–), 3.76–3.73 (*t*, $^3J_{HH}$ = 5.1 Hz, 2H, –CH_2–O), 3.61-3.58 (*sept*, $^3J_{HH}$ = 5.1 Hz, 1H, –CH), 2.41-2.34 (*m*, 8H, P–CH_2–), 1.48–1.46 (*m*, 16H, –CH_2–), 1.21–1.20, (*d*, $^3J_{HH}$ = 6.1 Hz, 6H, –CH_3) ppm. 0.84–0.87 (t, $3J_{HH}$ = 7.1 Hz, 12H, –CH_3) ppm. ^{13}C NMR (100.64 MHz, $CDCl_3$): 171.20, 163.58, 132.43, 121.78, 114.56, 72.47, 68.12, 66.45, 22.19. ^{31}P NMR (162.01 MHz, $CDCl_3$): 33.00 ppm.

(P_{4444})(3-IEBA): Pale yellow liquid. MS (ESI). $(C_{16}H_{36}P)^+$: Calcd m/z 259.2556. Found m/z 259.2569,, $[C_{12}H_{15}O_4]^-$: Calcd m/z 223.0975, Found m/z 223.0934. ^{1}H NMR (400.21 MHz, $CDCl_3$), $^\delta$(ppm): 7.67–7.65 (*m*, 2H), 7.20–7.16 (*m*,1H), 6.90–6.88 (*m*, 1H), 4.17–4.13 (*t*, $^3J_{HH}$ = 5.0 Hz, 2H, O–CH_2–), 3.78–3.75 (*t*, $^3J_{HH}$ = 6.11 Hz, 2H, –CH_2–O), 3.72–3.67 (*sept*, $^3J_{HH}$ = 6.6 Hz, 1H, -CH), 2.45-2.38 (*m*, 8H, P–CH_2–), 1.52-1.47 (*m*, 16H, –CH_2–), 1.20–1.18, (*t*, $^3J_{HH}$ = 5.2 Hz, 6H, –CH_3) ppm. 0.98–0.92 (t, $3J_{HH}$ = 3.5 Hz, 12H, –CH_3) ppm. ^{13}C NMR (100.64 MHz, $CDCl_3$): 171.48, 158.57, 142.61, 128.08, 122.25, 116.48, 114.71, 72.06, 67.86, 66.83, 24.21, 24.07, 24.06, 24.03, 22.27, 19.18, 18.17, 13.60. ^{31}P NMR (162.01 MHz, $CDCl_3$): 33.03 ppm.

(P_{4444})(4-IEBA): Pale yellow liquid. MS (ESI). $(C_{16}H_{36}P)^+$: Calcd m/z 259.2556. Found m/z 259.2565, $[C_{12}H_{15}O_4]^-$: Calcd m/z 223.0975, Found m/z 223.0934. ^{1}H NMR (400.21 MHz, $CDCl_3$), $^\delta$(ppm): 7.99–7.97 (*d*, $^3J_{HH}$ = 8.4 Hz, 2H), 6.82–6.80 (*d*, $^3J_{HH}$ = 8.4 Hz, 2H), 4.10–4.08 (*t*, $^3J_{HH}$ = 4.9 Hz, 2H, O–CH_2–), 3.77–3.64 (*m*, 2H), 1.42–1.40 (*m*, 16H, –CH_2–), 1.20–1.18, (*t*, $^3J_{HH}$ = 5.2 Hz, 6H, -CH_3) ppm. 0.98–0.92 (t, $3J_{HH}$ = 3.5 Hz, 12H, –CH_3) ppm. ^{13}C NMR (100.64 MHz, $CDCl_3$): 171.82, 160.00, 132.72, 131.14, 113.37, 116.48, 72.25, 67.77, 66.67, 24.10, 23.95, 23.89, 23.85, 22.19, 19.00, 18.53, 13.54. ^{31}P NMR (162.01 MHz, $CDCl_3$): 32.96 ppm.

(P_{4444})(2-EEBA): Pale yellow liquid. ^{1}H NMR (400.21 MHz, $CDCl_3$), $^\delta$(ppm): 7.45–7.43 (*d*, $^3J_{HH}$ = 7.2 Hz 1H), 7.09–7.05 (*d*, $^3J_{HH}$ = 7.9 Hz, 1H), 6.85–6.81 (*m*, 2H), 4.19–4.16 (*t*, $^3J_{HH}$ = 5.4 Hz, 2H, O–CH_2–), 3.76–3.73 (*t*, $^3J_{HH}$ = 5.3 Hz, 2H, –CH_2–O), 3.57-3.51 (*t*, $^3J_{HH}$ = 6.9 Hz, 2H), 2.39-2.36 (*m*, 8H, P–CH_2–), 1.46-1.44 (*m*, 16H, –CH_2–), 1.19–1.17, (*d*, $^3J_{HH}$ = 7 Hz, 3H, –CH_3) ppm. 0.84–0.87 (t, $3J_{HH}$ = 7.1 Hz, 12H, –CH_3) ppm. ^{13}C NMR (100.64 MHz, $CDCl_3$): 172.67, 155.29, 134.71, 129.02, 127.54, 120.93, 114.18, 69.32, 68.93, 66.88, 24.18, 24.03, 23.98, 19.01, 18.54, 15.41, 13.66. ^{31}P NMR (162.01 MHz, $CDCl_3$): 33.03 ppm.

(P_{4444})(2-MEMBA): Pale yellow liquid. MS (ESI). $(C_{16}H_{36}P)^+$: Calcd m/z 259.2556. Found m/z 259.2552, $[C_{13}H_{17}O_5]^-$: Calcd m/z 253.1081, Found m/z 253.1321. ^{1}H NMR (400.21 MHz, $CDCl_3$), $^\delta$(ppm): 7.43–7.41 (*m*, 1H), 7.08–7.04 (*m*, 1H), 6.83–6.79 (*m*, 2H), 4.17–4.15 (*t*, $^3J_{HH}$ = 5.2 Hz, 2H, O–CH_2–), 3.82-3.79 (*t*, $^3J_{HH}$ = 5.3 Hz, 2H, –CH_2–O), 3.68–3.66 (*t*, $^3J_{HH}$ = 4.3 Hz, 2H), 3.56–3.45 (*m*, 8H) 2.33–2.30 (*m*, 8H, P-CH_2–), 1.46–1.44 (*m*, 16H, –CH_2–), 1.19–1.17, (*d*, $^3J_{HH}$ = 7 Hz, 6H, –CH_3) ppm. 0.84–0.87 (t, $3J_{HH}$ = 7.1 Hz, 12H, –CH_3) ppm. ^{13}C NMR (100.64 MHz, $CDCl_3$): 172.78, 155.29, 134.42, 128.93, 127.67, 120.84, 114.51, 77.59, 77.28, 76.96, 70.77, 69.97, 68.88, 66.68, 24.13, 23.98, 23.95, 23.90 18.96, 18.49, 15.27, 13.61. ^{31}P NMR (162.01 MHz, $CDCl_3$): 33.04 ppm.

Nuclear Magnetic Resonance Spectroscopy: The structures and purity of all the synthesized products were confirmed by using a Bruker Ascend Aeon WB 400 (Bruker BioSpin AG, Fallanden, Switzerland) nuclear magnetic resonance (NMR) spectrometer. $CDCl_3$ was used as a solvent. The working frequencies were 400.21 MHz for ^{1}H, 100.64 MHz for ^{13}C, and 162.01 MHz for ^{31}P. Data were processed using Bruker Topspin 3.5 software.

Thermal Analysis: Thermogravimetric analysis (TGA) was performed using a PerkinElmer TGA 8000 under N_2 gas at a heating rate of 10 °C per min. About 2–4 mg of sample was used for each experiment. The onset of decomposition temperature, T_{onset}, was calculated from the intersection of the baseline weight and the tangent of the weight versus temperature curve using the Pyris software. Differential scanning calorimetry (DSC) was performed using a PerkinElmer DSC 6000 on 2–5 mg of the sample placed in an aluminum pan. DSC data were collected at a scanning rate of 5 °C min^{-1} for both cooling and heating traces. To maintain an inert environment inside the sample chamber, dry N_2 gas was delivered at a constant flow rate of 20 mL min^{-1}. The glass transition temperature (T_g) was determined by using the inflection mid-point of the initial *S*-shaped transition slope and determined from the onset with the aid of the Pyris software.

Electrochemical Characterization: The electrochemical stability and ionic conductivity were determined using a Metrohm Autolab PGSTAT302N electrochemical workstation with a FRA32 M module for impedance measurements, all controlled by a Nova 2.02 software. A sealed Microcell HC from RHD instruments Germany was used to hold about 70 μL of the sample. To determine the electrochemical stability window (ESW), linear sweep voltammetry (LSV) was performed with a three-electrode setup: a glassy carbon (GC) wire with a diameter of 2 mm as a working electrode (WE), a Pt crucible as counter electrode (CE) as well as a sample container, and an Ag wire coated with AgCl as a pseudo-reference electrode (RE). Both cathodic and anodic scans were recorded at a scan rate of 1 mV s^{-1}. The electrochemical potentials were calibrated using ferrocene (Fc) as an internal reference and shifted using $E_{Li/Li^+} \approx E_{Fc/Fc^+} + 3.2$ V.[60] The ESWs limits were defined by 0.1 mA cm^{-2} cut-off current density.

The ionic conductivity was obtained from the impedance measurements performed in a frequency range from 1 Hz to 1 MHz with an AC voltage amplitude of 10 mV_{rms}. All the impedance spectra were measured during heating and cooling over a temperature range from −20 to 100 ± 0.1 °C. A two-electrode configuration was employed for ionic conductivity measurements, with a wire Pt as a WE and a 70 μL Pt crucible as a sample container as well as CE.

Prior to each LSV and ionic conductivity measurement, both the electrodes were polished with a 0.25 m of Kemet diamond paste. The cell constant was calculated using a Metrohm 100 S cm^{-1} KCl standard solution (K_{cell} = 18.5396 cm^{-1}). The cell was thermally equilibrated for 10 minutes before recording the impedance spectra.

The relationship between temperature (*T*) and ion conductivity (σ) was fitted using the Vogel–Fulcher–Tammann (VFT) Equation (2).

$$\sigma = \sigma_0 \exp\left(\frac{-B}{(T - T_0)}\right) \quad (2)$$

Where σ_0 is a pre-exponential factor, *B* and T_0 are adjustable parameters, where the former is an empirical fitting parameter related to T_g and activation energy (E_a) of the system, and the latter is referred to the ideal vitreous transition temperature, at which configurational entropy vanishes.

NMR Diffusometry: Pulsed field gradient (PFG) NMR diffusometry measurements were performed using the same NMR spectrometer and a PFG NMR probe Diff50 (Bruker) with a maximum amplitude of the magnetic field gradient pulse of 29.73 T m^{-1}. The samples were placed in a standard 5 mm NMR glass tube and closed with a plastic stopper to avoid contact with air. Prior to measurements, each sample was equilibrated at a specific temperature for 30 min. The details of the PFG NMR technique for measuring molecular

diffusion coefficients are available elsewhere.[61] The diffusivity of a molecule is the diffusion decay (DD) of amplitude A of NMR spectral line, obtained by Fourier transformation of a descending half of stimulated-echo (StE), as a function of the amplitude of applied pulsed field gradient. For the stimulated echo pulse sequence used, diffusion decay of A in the case of simple non-associating molecular liquid can be described by Equation (3):[62]

$$A(g,\delta,t_d) = A(0)\exp(-\gamma^2 g^2 \delta^2 D t_d) \quad (3)$$

where $A(0)$ is the factor proportional to the proton content in the system, and to spin-lattice and spin-spin relaxation times, γ is the gyromagnetic ratio for a used nucleus; g and δ are the amplitude and duration of the gradient pulse; t_d is the diffusion time; and D is the self-diffusion coefficient. t_d was in the range 4–100 ms for ^{1}H diffusion and 5–15 ms for ^{7}Li diffusion. No diffusion time dependence was observed in these measurements.

The diffusivity data is analyzed by fitting into the following VFT Equation (4):

$$D = D_0 \exp\left(\frac{-B}{(T - T_0)}\right) \quad (4)$$

where D_0, T_0, B are adjustable parameters. Energy of activation for diffusion is related with B as $E_D = B \times R$. We have described $D(T)$ by fitting D_0, T_0 and B.

FTIR Spectroscopy: The attenuated total reflection Fourier transform infrared (ATR-FTIR) spectra were recorded using a Bruker IFS 80v spectrometer equipped with a deuterated triglycine sulfate (DTGS) detector and diamond ATR accessory, employing the double-side forward-backward acquisition mode. The total number of scans was 256, co-added and signal-averaged at an optical resolution of 4 cm^{-1}.

Acknowledgements

The financial support from the Swedish Energy Agency (project number: 48194-1) is gratefully acknowledged.

Conflict of Interests

The authors declare no conflict of interest.

Data Availability Statement

The data that support the findings of this study are available in the supplementary material of this article.

Keywords: flexible anions · fluorine-free electrolytes · ionic liquids · lithium-ion batteries · oligoether

[1] F. Wu, J. Maier, Y. Yu, *Chem. Soc. Rev.* **2020**, *49*, 1569–1614.
[2] L. Zhang, X. Li, M. Yang, W. Chen, *Energy Storage Mater.* **2021**, *41*, 522–545.
[3] Y. Zheng, Y. Yao, J. Ou, M. Li, D. Luo, H. Dou, Z. Li, K. Amine, A. Yu, Z. Chen, *Chem. Soc. Rev.* **2020**, *49*, 8790–8839.
[4] P. V. Chombo, Y. Laoonual, *J. Power Sources* **2020**, *478*, 228649.
[5] J. Duan, X. Tang, H. Dai, Y. Yang, W. Wu, X. Wei, Y. Huang, *Electrochem. Energy Rev.* **2020**, *3*, 1–42.
[6] J. Kalhoff, G. G. Eshetu, D. Bresser, S. Passerini, *ChemSusChem* **2015**, *8*, 2154–2175.
[7] H. Yang, G. V. Zhuang, P. N. Ross Jr, *J. Power Sources* **2006**, *161*, 573–579.
[8] S. F. Lux, J. Chevalier, I. T. Lucas, R. Kostecki, *ECS Electrochem. Lett.* **2013**, *2*, A121.
[9] K. Deng, Q. Zeng, D. Wang, Z. Liu, G. Wang, Z. Qiu, Y. Zhang, M. Xiao, Y. Meng, *Energy Storage Mater.* **2020**, *32*, 425–447.
[10] S. S. Zhang, *J. Power Sources* **2006**, *162*, 1379–1394.
[11] B. S. Lalia, N. Yoshimoto, M. Egashira, M. Morita, *J. Power Sources* **2010**, *195*, 7426–7431.
[12] A. Lewandowski, A. Świderska-Mocek, *J. Power Sources* **2009**, *194*, 601–609.
[13] S. Brutti, E. Simonetti, M. De Francesco, A. Sarra, A. Paolone, O. Palumbo, S. Fantini, R. Lin, A. Falgayrat, H. Choi, *J. Power Sources* **2020**, *479*, 228791.
[14] Y. Katayama, T. Morita, M. Yamagata, T. Miura, *Electrochemistry* **2003**, *71*, 1033–1035.
[15] P. C. Howlett, N. Brack, A. F. Hollenkamp, M. Forsyth, D. R. Macfarlane, *J. Electrochem. Soc.* **2006**, *153*, A595.
[16] A. Guerfi, S. Duchesne, Y. Kobayashi, A. Vijh, K. Zaghib, *J. Power Sources* **2008**, *175*, 866–873.
[17] W. Weng, Z. Zhang, J. Lu, K. Amine, *Chem. Commun.* **2011**, *47*, 11969–11971.
[18] R. McCallum, M. Barghamadi, C. Forsyth, A. F. Hollenkamp, G. Oldham, P. J. Mahon, T. Ruther, *J. Phys. Chem. C* **2021**, *125*, 8055–8067.
[19] X.-G. Sun, C. Liao, N. Shao, J. R. Bell, B. Guo, H. Luo, D.-e. Jiang, S. Dai, *J. Power Sources* **2013**, *237*, 5–12.
[20] M. A. Navarra, K. Fujimura, M. Sgambetterra, A. Tsurumaki, S. Panero, N. Nakamura, H. Ohno, B. Scrosati, *ChemSusChem* **2017**, *10*, 2496–2504.
[21] K. Kim, Y.-H. Cho, H.-C. Shin, *J. Power Sources* **2013**, *225*, 113–118.
[22] T. Yim, M. S. Kwon, J. Mun, K. T. Lee, *Isr. J. Chem.* **2015**, *55*, 586–598.
[23] D. L. Thompson, J. M. Hartley, S. M. Lambert, M. Shiref, G. D. Harper, E. Kendrick, P. Anderson, K. S. Ryder, L. Gaines, A. P. Abbott, *Green Chem.* **2020**, *22*, 7585–7603.
[24] D. Lisbona, T. Snee, *Process Saf. Environ. Prot.* **2011**, *89*, 434–442.
[25] F. U. Shah, O. I. Gnezdilov, I. A. Khan, A. Filippov, N. A. Slad, P. Johansson, *J. Phys. Chem. B* **2020**, *124*, 9690–9700.
[26] M. Forsyth, L. Porcarelli, X. Wang, N. Goujon, D. Mecerreyes, *Acc. Chem. Res.* **2019**, *52*, 686–694.
[27] X. Tang, S. Lv, K. Jiang, G. Zhou, X. Liu, *J. Power Sources* **2022**, *542*, 231792.
[28] F. Ilyas, M. Ishaq, M. Jabeen, M. Saeed, A. Ihsan, M. Ahmed, *J. Mol. Liq.* **2021**, *343*, 117606.
[29] C. Xu, G. Yang, D. Wu, M. Yao, C. Xing, J. Zhang, H. Zhang, F. Li, Y. Feng, S. Qi, *Chem. Asian J.* **2021**, *16*, 549–562.
[30] M. Armand, P. Johansson, M. Bukowska, P. Szczeciński, L. Niedzicki, M. Marcinek, M. Dranka, J. Zachara, G. Żukowska, M. Marczewski, *J. Electrochem. Soc.* **2020**, *167*, 070562.
[31] E. Hosseini-Bab-Anari, A. Boschin, T. Mandai, H. Masu, K. Moth-Poulsen, P. Johansson, *RSC Adv.* **2016**, *6*, 85194–85201.
[32] P. Jankowski, W. Wieczorek, P. Johansson, *Energy Storage Mater.* **2019**, *20*, 108–117.
[33] S. Bhowmick, M. Ahmed, A. Filippov, L. C. Loaiza, F. U. Shah, P. Johansson, *Chem. Commun.* **2023**, *59*, 2620–2623.
[34] M. Ahmed, S. S. Rao, A. Filippov, P. Johansson, F. U. Shah, *Phys. Chem. Chem. Phys.* **2023**, *25*, 3502–3512.
[35] D. Aurbach, E. Granot, *Electrochim. Acta* **1997**, *42*, 697–718.
[36] K. Westman, R. Dugas, P. Jankowski, W. Wieczorek, G. Gachot, M. Morcrette, E. Irisarri, A. Ponrouch, M. R. Palacín, J.-M. Tarascon, *ACS Appl. Energ. Mater.* **2018**, *1*, 2671–2680.
[37] S. Fang, G. Wang, L. Qu, D. Luo, L. Yang, S.-i. Hirano, *J. Mater. Chem. A.* **2015**, *3*, 21159–21166.
[38] K. Xu, *Chem. Rev.* **2004**, *104*, 4303–4418.
[39] J. G. Han, K. Kim, Y. Lee, N. S. Choi, *Adv. Mater.* **2019**, *31*, 1804822.
[40] F. U. Shah, I. A. Khan, P. Johansson, *Molecules* **2020**, *25*, 2388.
[41] I. A. Khan, O. I. Gnezdilov, A. Filippov, F. U. Shah, *ACS Sustainable Chem. Eng.* **2021**, *9*, 7769–7780.
[42] G. G. Botte, R. E. White, Z. Zhang, *J. Power Sources* **2001**, *97*, 570–575.
[43] G. M. Girard, M. Hilder, H. Zhu, D. Nucciarone, K. Whitbread, S. Zavorine, M. Moser, M. Forsyth, D. R. Macfarlane, P. C. Howlett, *Phys. Chem. Chem. Phys.* **2015**, *17*, 8706–8713.

[44] X. Gao, F. Wu, A. Mariani, S. Passerini, *ChemSusChem* **2019**, *12*, 4185–4193.
[45] S. Fang, Z. Zhang, Y. Jin, L. Yang, S.-i. Hirano, K. Tachibana, S. Katayama, *J. Power Sources* **2011**, *196*, 5637–5644.
[46] M. Galiński, A. Lewandowski, I. Stępniak, *Electrochim. Acta* **2006**, *51*, 5567–5580.
[47] K. Tsunashima, M. Sugiya, *Electrochem. Commun.* **2007**, *9*, 2353–2358.
[48] I. A. Khan, O. I. Gnezdilov, Y.-L. Wang, A. Filippov, F. U. Shah, *J. Phys. Chem. B.* **2020**, *124*, 11962–11973.
[49] K. J. Fraser, D. R. MacFarlane, *Aust. J. Chem.* **2009**, *62*, 309–321.
[50] R. Wibowo, S. E. W. Jones, R. G. Compton, *J. Chem. Eng. Data.* **2010**, *55*, 1374–1376.
[51] L. Gasparotto, N. Borisenko, N. Bocchi, S. Z. El Abedin, F. Endres, *Phys. Chem. Chem. Phys.* **2009**, *11*, 11140–11145.
[52] S. Kazemiabnavi, Z. Zhang, K. Thornton, S. Banerjee, *J. Phys. Chem. B.* **2016**, *120*, 5691–5702.
[53] N. De Vos, C. Maton, C. V. Stevens, *ChemElectroChem* **2014**, *1*, 1258–1270.
[54] A. Filippov, B. Munavirov, S. Glavatskih, F. U. Shah, O. N. Antzutkin, *Front. Chem.* **2020**, *8*, 119.
[55] T. Fromling, M. Kunze, M. Schonhoff, J. Sundermeyer, B. Roling, *J. Phys. Chem. B.* **2008**, *112*, 12985–12990.
[56] B. Gélinas, M. Natali, T. Bibienne, Q. P. Li, M. l. Dollé, D. Rochefort, *J. Phys. Chem. C* **2016**, *120*, 5315–5325.
[57] V. L. Martins, N. Sanchez-Ramirez, M. C. Ribeiro, R. M. Torresi, *Phys. Chem. Chem. Phys.* **2015**, *17*, 23041–23051.
[58] F. U. Shah, A. Holmgren, M. W. Rutland, S. Glavatskih, O. N. Antzutkin, *J. Phys. Chem. C.* **2018**, *122*, 19687–19698.
[59] R. Frech, W. Huang, *Macromolecules* **1995**, *28*, 1246–1251.
[60] A. R. Neale, S. Murphy, P. Goodrich, C. Hardacre, J. Jacquemin, *ChemPhysChem* **2017**, *18*, 2040–2057.
[61] P. T. Callaghan, *Principles of nuclear magnetic resonance microscopy*, Oxford University Press on Demand, **1993**.
[62] J. E. Tanner, *Chem. Phys.* **1970**, *52*, 2523–2526.

Manuscript received: March 29, 2023
Accepted manuscript online: May 5, 2023
Version of record online: May 5, 2023

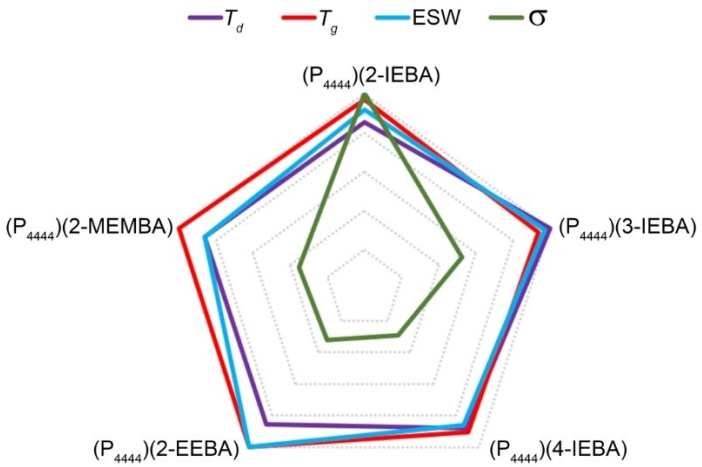

Structural analogous ionic liquids (ILs) and electrolytes comprising oligoether-based flexible aromatic anions offer different physicochemical properties. The designed ILs and the electrolytes are fluorine-free and have better physicochemical properties than conventional electrolytes and have a great potential to be used as electrolytes in next generation batteries, in particular those operating at elevated temperatures and with limited electrochemical stability window.

M. Ahmed, S. Bhowmick, A. Filippov, P. Johansson, F. U. Shah**